HHS Public Access

Author manuscript

ACS Appl Mater Interfaces. Author manuscript; available in PMC 2022 April 23.

Published in final edited form as:

ACS Appl Mater Interfaces. 2022 March 23; 14(11): 12964–12975. doi:10.1021/acsami.1c19617.

Ginger and Garlic Extracts Enhance Osteogenesis in 3D Printed Calcium Phosphate Bone Scaffolds with Bimodal Pore Distribution

Susmita Bose,

W.M. Keck Biomedical Materials Research Laboratory, School of Mechanical and Materials Engineering, Washington State University, Pullman, Washington 99164, United States

Dishary Banerjee,

W.M. Keck Biomedical Materials Research Laboratory, School of Mechanical and Materials Engineering, Washington State University, Pullman, Washington 99164, United States

Ashley A. Vu

W. M. Keck Biomedical Materials Research Laboratory, School of Mechanical and Materials Engineering, Washington State University, Pullman, Washington 99164, United States

Abstract

Natural medicines have long been used to treat physiological ailments where both ginger (gingerol) and garlic (allicin) are key players in immune system promotion, reduction in blood pressure, and lowering inflammation response. With their efficacy in bone healing, these compounds have great value as medicinal additives in bone scaffolds for localized treatment to support tissue formation, along with providing their natural therapeutic benefits. Utilization of 3D-printed (3DP) bone tissue engineering scaffolds as drug delivery vehicles for ginger and garlic extracts enables patient specificity in bone defect applications with enhanced osseointegration. Our objective is to understand their combined efficacy on osteogenesis when released from 3DP calcium phosphate bone scaffolds designed with a bimodal pore distribution. With a porous core and dense exterior, the resulting scaffolds have good mechanical integrity with 10 ± 1 MPa compressive strengths. Results show that ginger + garlic extracts released from bone scaffolds enhance their osteogenic potential through on site drug delivery. Both compounds exhibit exponential drug release profiles which fit Weibull distribution equations. The release of ginger extract also increases osteoblast proliferation by 59%. Both compounds show decreased

Corresponding Author: Susmita Bose – *W. M. Keck Biomedical Materials Research Laboratory, School of Mechanical and Materials Engineering, Washington State University, Pullman, Washington 99164, United States*; sbose@wsu.edu.

Author Contributions

D.B. and A.A.V. contributed equally to this work. S.B. secured funding and supervised the research.

ASSOCIATED CONTENT

Supporting Information

The Supporting Information is available free of charge at https://pubs.acs.org/doi/10.1021/acsami.1c19617.

Weibull distribution equation parameters for drug release; modified Masson-Goldner trichrome color analysis example of all compositions at 4 weeks; ginger and garlic extract H&E stain at 4 weeks; and color hue distribution for collagen analysis at 4 and 10 weeks (PDF)

Notes

The authors declare no competing financial interest.

Complete contact information is available at: https://pubs.acs.org/10.1021/acsami.1c19617

osteoclast resorption activity, with a greater than 20% reduction in pit area on sample surfaces. Ginger + garlic extract induces a twofold increase in early osteoid tissue formation *in vivo* at week 4, in addition to a 30% increase in total bone area and a 90% increase in osteocytes with respect to control 3DP tricalcium phosphate scaffolds. Late-stage bone healing at week 10 reveals healthy angiogenic tissue, a twofold higher bone mineralization, and significant enhancement of type I collagen formation in the presence of ginger and garlic extracts. Naturally sourced ginger and garlic extracts provide osteogenic promotion and improved bone tissue in-growth in a patient-specific 3DP scaffold biomedical device for low load-bearing bone tissue engineering and dental applications.

Graphical Abstract

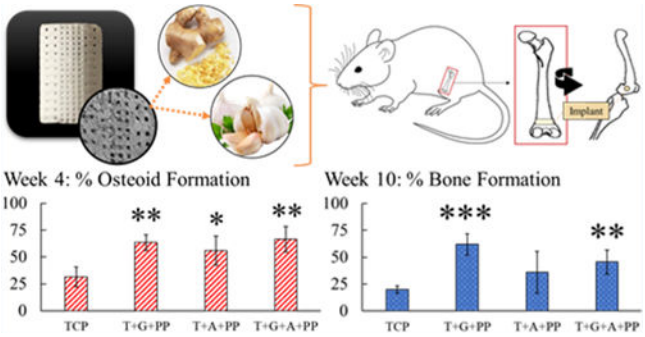

Keywords

ginger extract; garlic extract; 3D printing; natural medicinal compounds; tricalcium phosphate

INTRODUCTION

Naturopathy is used by one in five adults across the United States because its safer utilization and reduction in adverse reactions compared to synthetic medications.[1] With natural medicines having a prominence in history and are growing in popularity, the inspiration for this work is to combine natural therapeutics to enhance osteogenesis in bone tissue engineering applications. Current treatment for osteoporosis includes synthetic medications such as statins and bisphosphonates. Both medications have shown treatment concerns, including muscular problems, upper gastrointestinal problems, and increased risk of atypical fractures and fracture recurrence.[2,3] Naturopathy provides a viable alternative in treatment options toward bone health, with the bonus of other positive therapeutics. Oral administration or injections are standard methods of naturopathy delivery; however, with the advent of three-dimensional printing (3DP) technologies, patient-specific biomedical implants with on-site drug delivery can be achieved.

This work combines two natural medicinal compounds, ginger extract (gingerol) and garlic extract (allicin), incorporated into bone-like scaffolds built via additive manufacturing or 3DP. Ginger and garlic extracts are perennial herbs indigenous to Asia that exhibit medicinal qualities. We extracted these natural medicinal compounds from the ginger root and garlic powder, respectively, and then incorporated the drug extracts into scaffold matrices. Among

the materials studied are hydroxyapatite (HA),[4–6] in the form of dense discs to accurately study osteoclast resorption potential, as well as tricalcium phosphate (TCP), utilized as the base for our porous bioresorbable 3DP scaffolds.[7,8] These scaffolds are designed with the natural bone morphology in mind—a stronger, denser exterior like that of the cortical bone and the porous, spongy interior like that of the trabecular (cancellous) bone. This bimodal design achieves higher compressive strengths because of the denser structure while maintaining central interconnected porosity for cell proliferation, nutrient transport, and vascularization.[9] The durable and applicable mechanical strength of the scaffolds is imperative for handleability during surgery and the physiological location of implantation, where the scaffolds are expected to bear load within the compromised bone bed region. With the therapeutic release of ginger and garlic extracts, these crack-free scaffolds can enhance bone healing in patient-specific low load-bearing bone defect applications.

Macroscale delivery systems can be dictated through many mechanisms, including diffusion, affinity, and degradation.[10,11] Literature reports demonstrate the ability and viability of using ginger and garlic extracts in bone health applications, but utilization in 3DP bone scaffolds has yet to be explored. Ginger has been utilized in clinical trials to relieve pain from knee osteoarthritis.[12] Another study observed ginger extract preserved bone mineral density, suggesting a preventative mechanism of osteoclast activity along with anti-inflammatory properties through influencing the nuclear factor kappa light chain enhancer of the activated B cell (NF-$\kappa\beta$) pathway.[13] Little knowledge is known on the effects of garlic on bone health in humans; however, animal studies have shown that garlic can minimize bone loss through increasing estrogen levels.[14,15] Garlic has also been shown to reduce osteoclast bone resorption.[16] Both ginger and garlic can also provide antibacterial properties.[17,18] Given the potentials of these herbs as medicinal compounds for bone tissue healing, the objective of this study is to understand the combined effects of ginger and garlic extracts on bone tissue formation *in vivo* to aid patients with bone defects and enhance early-stage bone tissue osseointegration. An additional therapeutic benefit captured in this study is the assessment of antibacterial efficacy using ginger and garlic extracts to support the prevention of catastrophic infections that can occur from invasive surgeries found in orthopedic and dental applications.

Natural medicinal compounds tend to have low bioavailability due to their inherent hydrophobicity and degradation through the oral administration pathway. Calcium phosphate scaffolds can be employed in patient-specific defects which bypass the natural oral administration. The aid of a polymeric release system can also enhance bioavailability by increasing drug hydrophilicity. This system employs a combination of polycaprolactone (PCL) and polyethylene glycol (PEG) where PCL aids in the modulation of the release kinetics, whereas PEG provides the hydrophilic properties necessary to release the compounds into aqueous environments.[19] Garlic extract (allicin), specifically, is known to have poor stability, but the long-term health benefits are still widely studied.[20]

Extracted compounds are chemically assessed for their respective isomers and studied *in vitro* with osteoblast and osteoclast cells, the bone-forming and bone-remodeling cells, respectively. Additionally, the *Staphylococcus epidermidis* bacterial strain is used to assess the antibacterial properties of both extracted compounds. Furthermore, ginger and garlic

extracts are loaded separately and combined into these bimodal pore 3DP TCP scaffolds, followed by implantation into a bilateral, bicortical rat distal femur model. The novelty of this study lies with the implementation of natural medicinal compounds gingerol and allicin in a biomedical device, such as a patient-specific 3DP scaffold, toward osteogenesis for bone tissue engineering orthopedic and dental applications.

EXPERIMENTAL SECTION

Scaffold Fabrication and Characterization.

Scaffolds were fabricated utilizing synthesized β-TCP powder in a 3D powder bed printer (ExOne, Irwin, PA, USA). Specific synthesis and printing methods can be found in other studies.[21–24] Designed porosity within the scaffolds consists of a denser outer ring with higher porosity in the core resembling the structure of cortical and cancellous bones. All pores were designed as 400 μm squares, dispersed through the X and Y axis. Scaffolds were built layer-by-layer with an organic binder, cured for 1.5 h at 175 °C, air blown to reveal porosity, and sintered at 1250 °C for 2 h. Porosity was measured using Archimedes' principle, and compressive strength was assessed using a screw-driven testing machine (AG-IS, Shimadzu, Japan) equipped with a load cell of 50 kN and a constant crosshead speed of 0.33 mm/min. Scaffolds used in compressive strength testing measured approximately 7 mm height × 11 mm diameter. Scaffolds used in subsequent *in vivo* testing measured approximately 3 mm diameter × 5 mm height.

Drug Extractions from Ginger and Garlic.

Extraction of ginger extract from diced ginger root (30 g) was performed using an ethanolic Soxhlet apparatus for 48 h at approximately 80 °C. Ginger extract powder was yielded after evaporation of the ethanol solvent at 60 °C. Extraction of garlic extract was performed using dried garlic powder and vortexed for 1 min in filtered deionized (DI) water at an 8 mg/mL concentration. The extract was filtered through a 0.22 μm filter to remove all remnants and purify the drug solution for cell culture.

NMR Characterization of Ginger and Garlic Extracts.

Both ginger and garlic extractions were analyzed using proton nuclear magnetic resonance (^{1}H NMR) spectroscopy. Deuterated water was used to resuspend the ginger extract powder and supplement the aqueous garlic extract before testing in a Bruker DRX 400 MHz spectrometer. Ginger extract was also assessed using ^{13}C NMR spectroscopy within deuterated chloroform.

Scaffold Loading and Release Study of Ginger and Garlic Extracts.

Calcium phosphate scaffolds were loaded for *in vitro* release analysis, cell culture, and *in vivo*. For all loading, ginger and garlic extracts were loaded via drop-casting at 1000 μg (1 mg) each with a polymer mixture of 65:35 molar ratio of PCL (M_w = 14,000, Sigma-Aldrich, MO) and PEG (M_w = 8000, Sigma-Aldrich, MO) dissolved in acetone. For ginger extract specifically, a 50:50 PCL/PEG molar ratio was also assessed for comparison in drug-releasing efficacy and kinetics. Ultimately, all loading was completed using a 65:35 molar ratio. The polymer mixture was combined with each respective drug solution of

ginger extract, garlic extract, and an equal parts ginger + garlic extract mixture. HA discs used for *in vitro* release testing and the osteoclast cell culture were of 12 mm diameter × 2 mm height fabricated using a uniaxial press at 165 MPa for 2 min and sintered at 1250 °C for 2 h.

Drug release was performed in a simulated physiological environment of phosphate-buffered saline (PBS) at pH 7.4 and a constant shaking of 150 rpm at 37 °C. Release solutions were extracted, and new buffer was replenished at hourly and daily timepoints of approximately 3, 6, and 12 h and 1, 2, 3, 5, 7, 11, 14, 17, 20, and 25 days. The volume of the buffer used was 4 ml, and solutions extracted were assessed using a BioTek Synergy 2 SLFPTAD microplate reader (BioTek, Winooski, VT, USA) at absorbance values of 282 and 227 nm for ginger and garlic extracts, respectively. Standard curves for both drug solutions with known drug concentrations were employed to quantify each timepoint.

In Vitro Cell Materials Interaction with Ginger and Garlic Extracts.

Samples used in osteoblast and osteoclast cultures were autoclave sterilized at 121 °C for 1 h. All culture preparations and experimentation were performed in a sterile hood with culture plates incubated in a sterile incubator throughout the study. Appropriate media changes occurred every 3 days throughout the culture. Drug and polymer solutions were loaded post sterilization before cell seeding to minimize chemical decomposition. Control and treatment compositions of 3DP TCP, TCP + ginger extract + PCL/PEG (T + G + PP), TCP + garlic extract + PCL/PEG (T + A + PP), and TCP + ginger + garlic extract + PCL/PEG (T + G + A + PP) were employed in the osteoblast study. Human fetal osteoblast cells (1.19, ATCC, Manassas, VA) were cultured per manufacturer specifications and seeded onto TCP discs at a density of about 25,000 cells per sample. Osteoblast cell media comprised of Dulbecco's modified Eagle's medium and Ham's F12 medium (DMEM/F12, Sigma, St. Louis, MO) in equal parts with the supplementation of 1.2 mg/mL sodium bicarbonate and 0.3 mg/mL G418 (Sigma-Aldrich, St. Louis, MO) all mixed with sterilized DI water. In addition, 10% fetal bovine serum (FBS, ATCC, Manassas, VA) and 0.1% penicillin–streptomycin were also used to supplement the media. Osteoblast culture was incubated at 34 °C and 5% CO_2. To assess cell viability, MTT assay [3-(4,5-dimethylthiazol-2-yl)-2,5-diphenyltetrazolium bromide] was employed after 3, 7, and 11 days of culture. MTT solution of 100 μL was loaded onto all samples in the well in addition to 900 μL of cell media and then incubated for 1 h at 34 °C. The solution was removed, followed by the addition of 600 μL of the solubilizer composed of 10% Triton X-100, 0.1 N HCl, and isopropanol to dissolve the formazan crystals. This solution in 100 μL increments was moved to a 96-well plate and then read in a microplate reader at 570 nm.

Osteoclast cells (THP1 monocytes, ATCC, Manassas, VA) were cultured per manufacturer specifications and seeded onto HA discs at a density of about 25,000 cells per sample. Osteoclast growth media comprised of Roswell Park Memorial Institute (RPMI)-1640, 0.05 mM 2-mercaptoethanol, and 10% FBS. After seeding onto discs, growth media was switched to differentiation media throughout the rest of the culture. Differentiation media comprised of 40 ng/mL phorbol 12-myristate 13-acetate (Sigma-Aldrich, St. Louis, MO) and 10 ng/mL receptor activator of the nuclear factor κ-B ligand (RANKL) with RPMI-1640

and FBS. Osteoclast culture was incubated at 37 °C and 5% CO_2, and media was replaced every 3 days. The resorption pits were assessed after 10 days of culturing via ultrasonication of samples in 1 mL of 1 M NaCl solution mixed with 0.2% Triton X-100 to lyse cells. Samples were then rinsed and dehydrated using an ethanol series, followed by gold coating before imaging using a scanning electron microscope. The lifecycle of an osteoclast ranges from approximately 9 to 12 to up to 14 days, where 10 days are utilized in this study to assess osteoclast viability and resorption potential prior to the natural endpoint or apoptosis.

An antibacterial disc diffusion test was employed to assess the zone of inhibition with both ginger and garlic extract drug solutions. Both solutions, at a concentration of 1 mg/mL, were loaded into specialized paper and placed onto *S. epidermidis* inoculated agar plates (Carolina Biological Supply Company, Burlington, NC, USA). Rehydration of bacterial cells and test preparations were followed from manufacturer specifications. Incubation for 22 h at 37 °C was performed prior to imaging for the zone of inhibition.

Rat Distal Femur Model.

A bilateral, bicortical rat distal femur model was developed following the Institutional Animal Care and Use Committee (IACUC) protocol from Washington State University, Pullman, WA. Bicortical is defined as the cylindrical implant (3 mm diameter × 5 mm length) entering the lateral cortex through to the medial cortex. Twenty rats of 320–340 g weight, Sprague-Dawley breed (Envigo, Wilmington, MA, USA), underwent bilateral, bicortical distal femur surgery and were euthanized at timepoints of 4 and 10 weeks. Rats were held in individual cages in humidity- and temperature-controlled room on a 12 h cycle of light and dark. Surgical anesthesia included IsoFlo (Isoflurane, USP, Abbott Laboratories, North Chicago, IL, USA) with oxygen. Defects were made using increasing drill bit sizes up to 3 mm in diameter. Implant compositions included TCP, TCP + ginger extract (gingerol), TCP + garlic extract (allicin), and TCP + ginger + garlic extracts (gingerol + allicin). Post implantation, sutures, and staples were employed to close the incision. To minimize inflammation and facilitate pain control, meloxicam was administered subcutaneously for 3 days post operatively. Euthanasia was performed using an overdose of CO_2. Femurs were harvested and placed in 10% neutral-buffered formalin solution.

Histomorphology and Histochemical Analysis.

After 72 h of immersion in formalin, femurs were dehydrated using a series of ethanol and acetone, followed by embedding in Spurr's resin. Tissue cross-sections perpendicular to the axis of the cylindrical implant were obtained using a low-speed diamond saw. The tissue sections were fixed on glass slides, followed by a series of grinding and polishing to obtain a tissue thickness of less than 10 μm. Modified Masson-Goldner trichrome staining is used to assess osteoid formation and bone mineralization under light microscopy.

Cross-sectional tissue sections were also assessed using hematoxylin & eosin (H&E), von Willebrand factor (vWF), and collagen staining. Femurs were decalcified by immersion in 14% ethylenediaminetetraacetate solution for 12 weeks with solution change every 2–3 days. Samples were removed and embedded in paraffin, followed by sectioning of less than 10 μm using a microtome cutter and fixed on positively charged slides. Respective stains

were performed and observed under light microscopy. Areas where the scaffold has been removed during decalcification are observed as empty hole zones, and tissue images are collected near these areas. H&E is used for nonspecific tissue staining where hematoxylin is a basic dye that stains acidic structures in purple. Eosin is an acidic dye that stains basic structures shades of red or pink. vWF is a marker to detect endothelial cells and was stained using a blood vessel staining kit (ECM 590, Millipore, MA, USA) as per the manufacturer's instructions. The rabbit anti-vWF polyclonal antibody was used as the primary antibody, and antigen retrieval was carried out using a steamer at 60 °C using PBS. For collagen staining, anti-rat type I collagen antibody, clone 1F10C2, biotinylated, 1 mg/mL × 0.1 mL (Chondrex, WA, USA) was used as the primary antibody. The remaining steps were identical to the vWF protocol.

Histomorphometry was performed on the modified Masson-Goldner trichrome-stained sections and the H&E tissue stains of week 4 using Gimp 2.10.10. The software was used to separate trabecular bone tissue from bone marrow to calculate total bone formation. Additionally, collagen stain analysis was performed by isolating for red through hue saturation and black pixels were excluded from final pixel ratio assessment.

Statistical Analysis.

Statistical analysis was performed using an analysis of variance with post-hoc Tukey and reported as mean ± standard deviation. Data collection was completed in triplicates or higher with a p value < 0.05 considered significant and indicated by * compared to the control. Tests include scaffold characterizations, osteoblast MTT assay, and histomorphometry of *in vivo* tissue sections. At least two to three femurs were utilized per stain with at least five sections per femur analyzed.

RESULTS

Scaffold Characterization.

Triplicate testing of scaffolds (Figure 1) using Archimedes' principle reveals porosities of 50 ± 0.5% and compressive strengths of 10 ± 1 MPa. A scanning electron microscopy micrograph showcases macrolevel designed pores along with residual scaffold microporosities. These porosities facilitate drug loading and subsequent release as well as support cell attachment and tissue in-growth.

NMR Characterization of Ginger and Garlic Extracts.

Both drug extractions are characterized using proton ^{1}H NMR spectroscopy to identify the characteristic isomers of gingerol and allicin, the main bioactive compounds found in ginger and garlic, from the spectrum of extracted compounds (Figures 2 and 3). Within the ginger extract, the olefinic protons and C_5 alkyl moiety showcase the identification of gingerol and carbohydrates were also cataloged.[25,26] Isomers of gingerol were also identified in the ^{13}C NMR spectrum of the ginger extraction. Peaks at C-10, C-9, C-1, C-7, C-2, C-4, and C-5 along with $-OCH_3$ were identified. Within the garlic extraction, organosulfur compounds are identified, which indicate that structures such as allicin were extracted. Additionally, various acids, metabolites, and carbohydrates are identified.[27,28]

Release of Ginger and Garlic Extracts from 3DP Porous Scaffolds.

Release profiles of ginger and garlic extracts are generated which indicates successful release of both drugs from the scaffold matrix despite their hydrophobicity (Figure 4a,b). Most likely due to the instability of garlic extract (allicin), release in the buffer solution is only sustained up to 2 days, reaching to nearly 35% release without and 45% with PCL/PEG.[29,30] A higher ginger extract release at 50% using a 50:50 PCL/PEG molar ratio compared to only 25% with a 65:35 ratio is observed. This result is anticipated due to the higher PEG usage in 50:50 which increases the overall hydrophilicity of ginger extract. A 65:35 PCL/PEG molar ratio is ultimately used for the remainder of the work because of the higher drug release seen using a 50:50 ratio and the maintenance of drug release consistency with 65:35.

The release of both drugs with and without the PCL/PEG polymer system shows an exponential release profile which follows the Weibull distribution equation:[29,30]

$$m = 1 - \exp\left[-\frac{(t)^b}{a}\right] \quad (1)$$

Where m is amount of drug released (Q = 100%*m), a is the time constant, and b is the shape parameter.

The Weibull distribution plots and equation factors can be found in the Supporting Information for all drug release plots (Figure S1). The non-linear regression criterion value R^2 obtained for the 50:50 polymer ratio for ginger extract shows 0.9460. The R^2 value shows 0.9836 in the case of ginger extract with 65:35 polymer ratio. Similarly, for garlic extract the obtained R^2 value was 0.9615 and 0.9825 with and without 65% PCL/PEG respectively. In summary, the R^2 values are > 0.9 for all compositions which indicates a good fit with a narrow confidence interval.

In Vitro Cell Materials Interaction with Ginger and Garlic Extracts.

Osteoblast cell viability (MTT assay) shows a significant increase in optical density (OD) with samples loaded with ginger extract compared to just TCP or with garlic extract at day 7 (Figure 4c). Ginger extract with PCL/PEG (G + PP) and ginger + garlic extract with PCL/PEG (G + A + PP) result in a 59 and 27% increase in OD, respectively, at day 7. This result indicates that ginger extract can enhance osteoblast cell proliferation in early timepoints. Additionally, all compositions did show an increase in OD by day 11. Following osteoclast culture, images show that ginger and garlic extracts can reduce resorption pits in severity, shape, size, and frequency (Figure 4d). Antibacterial testing revealed antibacterial properties for both ginger and garlic extracts via a clear zone of inhibition surrounding the paper disc as opposed to no ring formed from the control (Figure 4e).

Histomorphology and Histochemical Analysis.

Following surgical implantation and harvesting of femurs (Figure 5a), Masson-Goldner trichrome for osteogenic tissue, H&E for bone tissue growth, vWF for blood vessel formation, and collagen-staining procedures are employed to perform histomorphology

and histochemical analysis. Week 4 color analysis of five images per composition of Masson-Goldner shows a significant trend of enhanced osteoid formation with ginger extract (gingerol), garlic extract (allicin), and both in combination (gingerol + allicin) (Figure 5b). An illustration of the color analysis for a set of week 4 images has been included in the Supporting Information (Figure S2). Optical microscopy images of the modified Masson-Goldner trichrome staining show prominent osteoid formation in ginger + garlic extract-loaded implants compared to the control (Figure 5c). H&E staining reveals healthy bone tissue, trabecular bone tissue, osteocytes, and bone marrow in all compositions (Figures 5d and S3). Tissue sections of the cancellous bone reveal bone marrow, stained in purple, and trabeculae bone tissue, stained in pink. Using image analysis to quantify the trabecular/bone tissue formation reveals that ginger + garlic extract can induce about 83% of total bone area of trabecular bone formation, whereas control TCP scaffolds only support nearly 57% total bone formation. This is also supported by the number of osteocytes seen in each respective tissue samples where ginger + garlic extract shows nearly 80 osteocytes, whereas control TCP shows only 40 osteocytes within a specific area of tissue. Collagen staining reveals an increase of collagen formation in ginger extract and even more collagen formation with ginger + garlic extract-loaded samples compared to control in week 4 (Figure 5e).

In week 10, there is higher mineralized bone formation with ginger extract and ginger + garlic extract scaffolds compared to the control and garlic extract (Figure 6a). Based on the color analysis, ginger extract and ginger + garlic extract do show a significantly higher percentage of bone mineralization compared to the control (Figure 6b). Ginger + garlic extract also shows a significantly higher osteoid formation at week 10 compared to the control. An increase in bone mineralization indicates an accelerating maturation of the bone. There are also prominent gaps in tissue growth, approximately 170–200 μm around the circumference of the implant at week 4, with control TCP scaffolds compared to ginger + garlic extract scaffolds. Gaps are still seen in the control at week 10 but less prominent. Healthy tissue seen in H&E staining is similarly comparable in all compositions at week 10 (Figure 6c). A recurring prominent presence of collagen in ginger + garlic extract is observed at week 10 (Figure 6d). Quantification of the collagen stain shows a significant increase between week 4 and week 10 for garlic extract-treated 3DP TCP scaffolds (Figure 6e). Methods of the color analysis can be viewed in the Supporting Information (Figure S4). To assess blood vessel formation, vWF stain is utilized where the vascular endothelial growth factor (VEGF) protein is one of the multiple growth factors that are tagged which signal support for osteogenesis and bone formation (Figure 7a). Indicated by red arrows, vWF staining showcases angiogenic support in the control TCP scaffold as well as TCP scaffolds loaded with ginger extract, garlic extract, and ginger + garlic extract (Figure 7b).

DISCUSSION

Surgical patients receiving procedures such as craniomaxillofacial, dental, and other bone void fillings due to defects or tumor resection would benefit from these patient-specific multi-therapeutic scaffolds. The bimodal distribution of pores embedded in the scaffold matrix better models bone architecture than previous works exploring uniform porosity.[21,22,31] With the denser outer core feature, compressive strength is reinforced, achieving 10 ± 1 MPa. This nears the higher end of cancellous bone strength,

approximately between 2 and 15 MPa, in addition to supporting proper tissue in-growth and vascularization.[9]

The rapid metabolism and elimination of natural medicinal compounds in the physiological environment hinder their practical application *in vivo.* Other methods to enhance bioavailability have been studied such as a nano transdermal delivery system for gingerol and powder supplements for garlic.[32,33] However, limited literature leaves further clinical and animal studies necessary to support the use of gingerol and allicin in pharmaceutical applications.[34] Results from this study reveal that an effective release of ginger and garlic extracts from porous 3DP TCP scaffolds *in vivo* is achievable, with improved bone healing in a rat distal femur model. Release of drugs from calcium phosphate matrices is a viable delivery vehicle to enhance drug bioavailability.[35] In addition, the utilization of PEG in this system enables the release of ginger extract (gingerol) that was otherwise not present at all. Previous reports from our group have shown the efficacy of a thin layer of PCL on controlling drug release.[19,29,36] Ginger extract, with the aid of PCL and PEG polymer nanocarriers, is released via hydrolytic reactions cleaving the bonds in the ginger extract-polymer conjugate system with rate dictated by the rate of these cleavages.[30] A 30% higher molar utilization of PEG increases release by nearly 4x in the initial stages up to 7 days and a 30% increase over the prolonged release. Drug release is dictated by many factors including environment, material, biological, and physicochemical reactions where drug release profiles can exhibit exponential or polynomial release mechanisms.[11,37] Ginger extract exhibits a Weibull distribution governed by different factors like drug diffusion, polymer degradation, drug-polymer and drug-substrate interactions, hydrophilicity, and porosity.[38–40] Garlic extract also exhibits a Weibull exponential distribution with and without PCL/PEG. Garlic extract has low hydrophilicy but enough to sustain a water solvent-based release, and this diffusion into water along with the above-mentioned factors, can lead to exponential release kinetics which fit a Weibull distribution. With the aid of PCL/PEG, this stabilized release is able to be sustained for twice as long than without a polymer drug carrier.

From the *in vivo* study employing a rat distal femur model, color quantification of the Masson-Goldner staining reveals that ginger and garlic extracts, individually and together, can significantly enhance early-stage osteoid formation at week 4 and bone mineralization at week 10. By week 4, the combined effects of ginger and garlic extracts also show high bone ingrowth, corroborated by an increase in the total bone area in the H&E staining. Image analysis reveals an increase in the trabecular bone formation by 30% and an increase in osteocytes by over 90%. The trabecular bone, also known as cancellous, porous, or spongy bone, is the surrounding tissue of pores and voids. If ginger and garlic extracts can induce higher trabecular bone tissue formation, a higher bone mineral density would be achieved from the lowered pore or void volume. By week 10, osseous tissue maturation is seen by the higher mineralized bone formation by the combined effects of ginger and garlic extracts compared to all other compositions. This improvement in osteogenesis could be attributed to the increase in bone formation brought forth by ginger extract and the reduction in bone resorption by ginger and garlic extracts, as the *in vitro* cell cultures suggest.

Osteoblast cells are the bone-forming cells used to lay new bone tissue and osteoclast cells remodel or remove old tissue.[41] Ginger extract shows a 59% increase in osteoblast proliferation, but ginger + garlic extract shows only a 27% increase in osteoblast formation. Knowing that garlic extract is an unstable compound,[20] it is possible that ginger and garlic extracts have interacted with one another, causing the ~30% decrease. Nevertheless, ginger extract shows an improvement in cellular viability which is corroborated by another work reporting enhanced bone formation and a reduction in bone loss with vertebral microarchitecture.[42] Reduced osteoclast resorption pits and reduced overall osteoclast activity are also found in this work utilizing ginger extract as well as garlic extract. The employment of ginger extract has various explanations for the attrition in osteoclastogenesis including influencing the inflammatory response NF-$\kappa\beta$ pathway, suppressing the interleukin (IL)-1-induced prostaglandin E_2 (PGE_2) production in osteoblasts, or affecting the RANK ligand expression in osteoblast cells.[13,43,44] The decreased osteoclastogenesis via garlic extract implementation does not have a defined mechanism of action within the literature but has been attributed to increased estrogen levels *in vivo*.[14–16]

Other observations which further support the osteogenic potential of ginger and garlic extracts *in vivo* are the well-supported blood vessel formation identified in all compositions as well as the increase in collagen seen by garlic extract-loaded scaffolds by week 10. Type I collagen is the most abundant collagen found in the human body and is the major component in bone, skin, tendons, ligaments, and other tissues.[45] Ginger extract has been reported to increase the expression of collagen, type I, alpha I (COL1A1), the gene expressed by type I collagen.[46] Moreover, there are three types of collagen: hyaline, fibro, and elastic. Unlike the other types of cartilage which are only made of type II collagen, fibrocartilage is mostly composed of type I collagen.[47,48] All cartilage contains chondrocytes which are the cells necessary for the maintenance of cartilage.[49] One study reported that garlic extract significantly promoted chondrocyte cell viability.[50] These results elucidate that garlic extract promotes type I collagen formation by enhancing chondrocytes within fibrocartilage. Type I collagen has been shown to induce osteoblastic differentiation of bone marrow cells, and this was assessed by higher alkaline phosphatase activity.[51] An increase in osteoblast differentiation, via the enhanced collagen formation by ginger + garlic extract, would enhance bone formation and thus improve bone healing.

Bacterial infection is a common problem for medical implants of which *S. epidermidis,* a Gram-positive bacterium, has affected prosthetics, catheters, breast, and orthopedic implants. This work reveals the antibacterial efficacies of both ginger and garlic extracts to aid in secondary infection control postsurgery. Secondary infections occur months after a surgery and is the cause of costly replacement or revision surgeries. Debridement of scar tissue from an infection, leading to complete implant removal, also poses large risk for secondary infections.[52] Utilizing ginger and garlic extracts can provide a natural treatment for infection prevention.[17,18]

CONCLUSIONS

In summary, 3DP TCP bioresorbable scaffolds with a bimodal porosity structure can enhance the drug bioavailability of ginger (gingerol) and garlic (allicin) extracts to enhance osteogenesis. With the denser outer core to mimic natural bone morphology, these scaffolds have a compressive strength comparable to cancellous bones at 10 ± 1 MPa. Drug release profiles of ginger and garlic extracts are fitted to a Weibull exponential distribution. Ginger and garlic extracts support osteoblast formation, with ginger extract inducing a 59% increase in osteoblast proliferation. These compounds also reduce osteoclast resorption activity by over 20%. In a rat distal femur model, ginger + garlic extract improves osteogenesis and enhance bone tissue in-growth. Results show a 30% increase in the total bone area and a 90% increase in osteocytes. Higher bone mineralization, total bone formation, angiogenic tissue, and enhancement of type I collagen formation are also observed at week 10. Our study shows the combined efficacy of the extracted compounds on osteogenesis, and while gingerol and allicin play key but differing roles in bone remodeling, they additionally provide individually distinct natural therapeutic benefits. In tandem, these compounds can bring more significant beneficiary and therapeutic range for clinical bone-healing applications. This work provides a multitherapeutic system for personalized medicine in patient-specific bone defects using nonimmunogenic, natural medicinal compounds.

Supplementary Material

Refer to Web version on PubMed Central for supplementary material.

ACKNOWLEDGMENTS

Authors would like to acknowledge financial support from the National Institutes of Health under the grant numbers R01 AR066361 and R01 DE029204-01. A special thanks to Yongdeok Jo and Ujjayan Majumdar for their assistance with release kinetic analysis as well as the Franceschi Microscopy & Imaging Center, Murdock Charitable Trust, and WSU NMR Center for their services. This content is solely the responsibility of the authors and does not necessarily represent the official views of the National Institutes of Health.

REFERENCES

(1). Noé JE L-Glutamine use in the Treatment and Prevention of Mucositis and Cachexia: Naturopathic Perspective. Integr. Cancer Ther. 2009, 8, 409–415. [PubMed: 19942578]

(2). Ganga HV; Slim HB; Thompson PD A Systematic Review of Statin-Induced Muscle Problems in Clinical Trials. Am. Heart J. 2014, 168, 6–15. [PubMed: 24952854]

(3). Lloyd AA; Gludovatz B; Riedel C; Luengo EA; Saiyed R; Marty E; Lorich DG; Lane JM; Ritchie RO; Busse B; Donnelly E Atypical Fracture with Long-Term Bisphosphonate Therapy is Associated with Altered Cortical Composition and Reduced Fracture Resistance. Proc. Natl. Acad. Sci. U.S.A. 2017, 114, 8722–8727. [PubMed: 28760963]

(4). Bhumiratana S; Grayson WL; Castaneda A; Rockwood DN; Gil ES; Kaplan DL; Vunjak-Novakovic G Nucleation and Growth of Mineralized Bone Matrix on Silk-Hydroxyapatite Composite Scaffolds. Biomaterials 2011, 32, 2812–2820. [PubMed: 21262535]

(5). Yuca E; Karatas AY; Seker UOS; Gungormus M; Dinler-Doganay G; Sarikaya M; Tamerler C In Vitro Labeling of Hydroxyapatite Minerals by an Engineered Protein. Biotechnol. Bioeng. 2011, 108, 1021–1030. [PubMed: 21190171]

(6). Vahabzadeh S; Roy M; Bandyopadhyay A; Bose S Phase Stability and Biological Property Evaluation of Plasma Sprayed Hydroxyapatite Coatings for Orthopedic and Dental Applications. Acta Biomater. 2015, 17, 47–55. [PubMed: 25638672]

(7). Ke D; Bose S Effects of Pore Distribution and Chemistry on Physical, Mechanical, and Biological Properties of Tricalcium Phosphate Scaffolds by Binder-Jet 3D Printing. Addit. Manuf 2018, 22, 111–117.

(8). Vallet-Regí M; Balas F; Arcos D Mesoporous Materials for Drug Delivery. Angew. Chem., Int. Ed. 2007, 46, 7548–7558.

(9). Barba A; Maazouz Y; Diez-Escudero A; Rappe K; Espanol M; Montufar EB; Öhman-Mägi C; Persson C; Fontecha P; Manzanares M-C; Franch J; Ginebra M-P Osteogenesis by Foamed and 3D-Printed Nanostructured Calcium Phosphate Scaffolds: Effect of Pore Architecture. Acta Biomater. 2018, 79, 135–147. [PubMed: 30195084]

(10). Bose S; Sarkar N Natural Medicinal Compounds in Bone Tissue Engineering. Trends Biotechnol. 2020, 38, 404–417. [PubMed: 31882304]

(11). Kearney CJ; Mooney DJ Macroscale Delivery Systems for Molecular and Cellular Payloads. Nat. Mater. 2013, 12, 1004–1017. [PubMed: 24150418]

(12). Altman RD; Marcussen KC Effects of a Ginger Extract on Knee Pain in Patients with Osteoarthritis. Arthritis Rheumatol. 2001, 44, 2531–2538.

(13). Funk JL; Frye JB; Wright LE; Timmermann BN Effects of Ginger (Zingiber officialis L) on Inflammation-Induced Bone Loss. Faseb. J. 2012, 26, 263.5.

(14). Mukherjee M; Das AS; Das D; Mukherjee S; Mitra S; Mitra C Role of Oil Extract of Garlic (Allium sativum Linn.) on Intestinal Transference of Calcium and its Possible Correlation with Preservation of Skeletal Health in an Ovariectomized Rat Model of Osteoporosis. Phytother Res. 2006, 20, 408–415. [PubMed: 16619371]

(15). Mukherjee M; Das AS; Das D; Mukherjee S; Mitra S; Mitra C Role of Peritoneal Macrophages and Lymphocytes in the Development of Hypogonadal Osteoporosis in an Ovariectomized Rat Model: Possible Phytoestrogenic Efficacy of Oil Extract of Garlic to Preserve Skeletal Health. Phytother Res. 2007, 21, 1045–1054. [PubMed: 17600860]

(16). Muhlbauer RC; Li F Effect of Vegetables on Bone Metabolism. Nature 1999, 401, 343–344. [PubMed: 10517630]

(17). Kim H-S; Lee SH; Byun Y; Park HD 6-Gingerol Reduces Pseudomonas Aeruginosa Biofilm Formation and Virulence via Quorum Sensing Inhibition. Sci. Rep. 2015, 5, 8656. [PubMed: 25728862]

(18). Durairaj S; Srinivasan S; Lakshmanaperumalsamy P In Vitro Antibacterial Activity and Stability of Garlic Extract at Different pH and Temperature. Electron. j. biol. 2009, 5, 5–10.

(19). Bose S; Sarkar N; Banerjee D Effects of PCL, PEG and PLGA Polymers on Curcumin Release from Calcium Phosphate Matrix for in Vitro and in Vivo Bone Regeneration. Mater. Today Chem. 2018, 8, 110–120. [PubMed: 30480167]

(20). Fujisawa H; Suma K; Origuchi K; Kumagai H; Seki T; Ariga T Biological and Chemical Stability of Garlic-Derived Allicin. J. Agric. Food Chem. 2008, 56, 4229–4235. [PubMed: 18489116]

(21). Bose S; Banerjee D; Robertson S; Vahabzadeh S Enhanced in Vivo Bone and Blood Vessel Formation by Iron Oxide and Silica Doped 3D Printed Tricalcium Phosphate Scaffolds. Ann. Biomed. Eng. 2018, 46, 1241–1253. [PubMed: 29728785]

(22). Vu AA; Bose S Vitamin D 3 Release from Traditionally and Additively Manufactured Tricalcium Phosphate Bone Tissue Engineering Scaffolds. Ann. Biomed. Eng. 2020, 48, 1025–1033. [PubMed: 31168676]

(23). Fielding G; Bose S SiO2 and ZnO Dopants in Three-Dimensionally Printed Tricalcium Phosphate Bone Tissue Engineering Scaffolds Enhance Osteogenesis and Angiogenesis in Vivo. Acta Biomater. 2013, 9, 9137–9148. [PubMed: 23871941]

(24). Banerjee SS; Tarafder S; Davies NM; Bandyopadhyay A; Bose S Understanding the Influence of MgO and SrO Binary Doping on the Mechanical and Biological Properties of β-TCP Ceramics. Acta Biomater. 2010, 6, 4167–4174. [PubMed: 20493283]

(25). Gan Z; Liang Z; Chen X; Wen X; Wang Y; Li M; Ni Y Separation and Preparation of 6-gingerol from Molecular Distillation Residue of Yunnan Ginger Rhizomes by High-Speed Counter-Current Chromatography and the Antioxidant Activity of Ginger Oils in Vitro. J. Chromatogr. B: Anal. Technol. Biomed. Life Sci 2016, 1011, 99–107.

(26). Zhan K; Xu K; Yin H Preparative Separation and Purification of Gingerols from Ginger (Zingiber officinale Roscoe) by High-Speed Counter-Current Chromatography. Food Chem. 2011, 126, 1959–1963. [PubMed: 25213983]

(27). Ritota M; Casciani L; Han B-Z; Cozzolino S; Leita L; Sequi P; Valentini M Traceability of Italian Garlic (Allium Sativum L.) by Means of HRMAS-NMR Spectroscopy and Multivariate Data Analysis. Food Chem. 2012, 135, 684–693. [PubMed: 22868146]

(28). Macpherson LJ; Geierstanger BH; Viswanath V; Bandell M; Eid SR; Hwang S; Patapoutian A The Pungency of Garlic: Activation of TRPA1 and TRPV1 in Response to Allicin. Curr. Biol. 2005, 15, 929–934. [PubMed: 15916949]

(29). Mendyk A; Jachowicz R; Fijorek K; Dorozynski P.la.; Kulinowski P; Polak S KinetDS: An Open Source Software for Dissolution Test Data Analysis. Dissolution Technology 2012, 19, 6–11.

(30). Gomes Filho MS; Oliveira FA; Barbosa MAA A Statistical Mechanical Model for Drug Release: Investigations on Size and Porosity Dependence. Physica A: Statistical Mechanics and its Applications 2016, 460, 29–37.

(31). Sarkar N; Bose S Liposome-Encapsulated Curcumin-Loaded 3D Printed Scaffold for Bone Tissue Engineering. ACS Appl. Mater. Interfaces 2019, 11, 17184–17192. [PubMed: 30924639]

(32). Baskar V; Selvakumar K; Madhan R; Srinivasan G; Muralidharan M Study on Improving Bioavailability Ratio of Anti-Inflammatory Compound from Ginger through Nano Transdermal Delivery. Asian J. Pharmaceut. Clin. Res. 2012, 5, 241–246.

(33). Lawson L; Hunsaker S Allicin Bioavailability and Bioequivalence from Garlic Supplements and Garlic Foods. Nutrients 2018, 10, 812.

(34). Shouk R; Abdou A; Shetty K; Sarkar D; Eid AH Mechanisms Underlying the Antihypertensive Effects of Garlic Bioactives. Nutr. Res. 2014, 34, 106–115. [PubMed: 24461311]

(35). Tarafder S; Banerjee S; Bandyopadhyay A; Bose S Electrically Polarized Biphasic Calcium Phosphates: Adsorption and Release of Bovine Serum Albumin. Langmuir 2010, 26, 16625–16629. [PubMed: 20939493]

(36). Banerjee D; Bose S Effects of Polymer Chemistry, Concentration, and pH on Doxorubicin Release Kinetics from Hydroxyapatite-PCL-PLGA Composite. J. Mater. Res. 2019, 34, 1692–1703.

(37). Maderuelo C; Zarzuelo A; Lanao JM Critical Factors in the Release of Drugs from Sustained Release Hydrophilic Matrices. Journal of Controlled Release 2011, 154, 2–19. [PubMed: 21497624]

(38). Fosca M; Rau JV; Uskokovic V Factors Influencing the Drug Release from Calcium Phosphate Cements. Bioactive Materials 2022, 7, 341–363. [PubMed: 34466737]

(39). Kobryn J; Sowa S; Gasztych M; Drys A; Musial W Influence of Hydrophilic Polymers on the Factor in Weibull Equation Applied to the Release Kinetics of a Biologically Active Complex of Aesculus Hippocastanum. International Journal of Polymer Science 2017, 2017, 1.

(40). Gbureck U; Vorndran E; Barralet JE Modeling Vancomycin Release Kinetics from Microporous Calcium Phosphate Ceramics Comparing Static and Dynamic Immersion Conditions. Acta Biomaterialia 2008, 4, 1480–1486. [PubMed: 18485844]

(41). Roy M; Bose S Osteoclastogenesis and Osteoclastic Resorption of Tricalcium Phosphate: Effect of Strontium and Magnesium Doping. J. Biomed. Mater. Res., Part A 2012, 100, 2450–2461.

(42). Zammel N; Amri N; Chaabane R; Rebai T; Badraoui R Proficiencies of Zingiber Officinale Against Spine Curve and Vertebral Damage Induced by Corticosteroid Therapy Associated with Gonadal Hormone Deficiency in a Rat Model of Osteoporosis. Biomed. Pharmacother. 2018, 103, 1429–1435. [PubMed: 29864927]

(43). Hwang Y-H; Kim T; Kim R; Ha H The Natural Product 6-Gingerol Inhibits Inflammation-Associated Osteoclast Differentiation via Reduction of Prostaglandin E2 Levels. Int. J. Mol. Sci. 2018, 19, 2068.

(44). Ito S; Ohmi A; Sakamiya A; Yano T; Okumura K; Nishimura N; Kagontani K Ginger Hexane Extract Suppresses RANKL-Induced Osteoclast Differentiation. Biosci., Biotechnol., Biochem. 2016, 80, 779–785. [PubMed: 26967638]

(45). Reddi AH; Gay R; Gay S; Miller EJ Transitions in Collagen Types During Matrix-Induced Cartilage, Bone, and Bone Marrow Formation. Proc. Natl. Acad. Sci. U.S.A. 1977, 74, 5589–5592. [PubMed: 271986]

(46). Han HS; Kim KB; Jung JH; An IS; Kim YJ; An S Anti-Apoptotic, Antioxidant and Anti-Aging Effects of 6-Shogaol on Human Dermal Fibroblasts. Biomed. dermatol 2018, 2, 27.

(47). Roberts S; Menage J; Sandell LJ; Evans EH; Richardson JB Immunohistochemical Study of Collagen Types I and II and Procollagen IIA in Human Cartilage Repair Tissue Following Autologous Chondrocyte Implantation. Knee 2009, 16, 398–404. [PubMed: 19269183]

(48). Benjamin M; Evans EJ Fibrocartilage. J. Anat. 1990, 171, 1. [PubMed: 2081696]

(49). Roughley P Articular Cartilage and Changes in Arthritis: Noncollagenous Proteins and Proteoglycans in the Extracellular Matrix of Cartilage. Arthritis Res. Ther. 2001, 3, 342.

(50). Li T; Shi HY; Hua YX; Gao C; Xia Q; Yang G; Li B Effects of Allicin on the Proliferation and Cell Cycle of Chondrocytes. Int. J. Clin. Exp. Pathol. 2015, 8, 12525. [PubMed: 26722440]

(51). Mizuno M; Fujisawa R; Kuboki Y Type I Collagen-Induced Osteoblastic Differentiation of Bone-Marrow Cells Mediated by Collagen-α2β1 Integrin Interaction. J. Cell. Physiol. 2000, 184, 207–213. [PubMed: 10867645]

(52). Campoccia D; Montanaro L; Arciola CR The Significance of Infection Related to Orthopedic Devices and Issues of Antibiotic Resistance. Biomaterials 2006, 27, 2331–2339. [PubMed: 16364434]

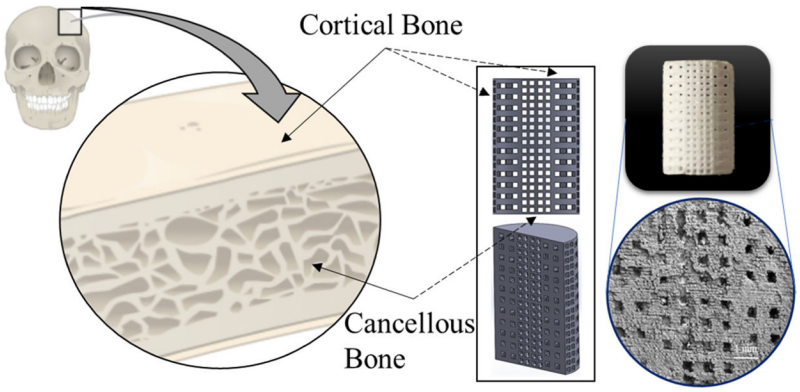

Figure 1.

Bimodal pore distribution bone scaffold. Interconnected porosity 3DP scaffolds are modeled after bone morphology and manufactured using powder bed binder jet printing. Bone contains cortical and trabecular bones (dense and spongy bones) which was the basis for the scaffold design used in this study. This bimodal pore distribution aids in increased mechanical properties by employing a dense exterior with a sustained interconnected porous interior that still allows for cell motility, nutrient flow, and vascularization. Dimensions of scaffolds are 7 mm diameter by 11 mm height for mechanical strength testing and 3 mm diameter by 5 mm height for *in vivo* implantation in a rat distal femur model.

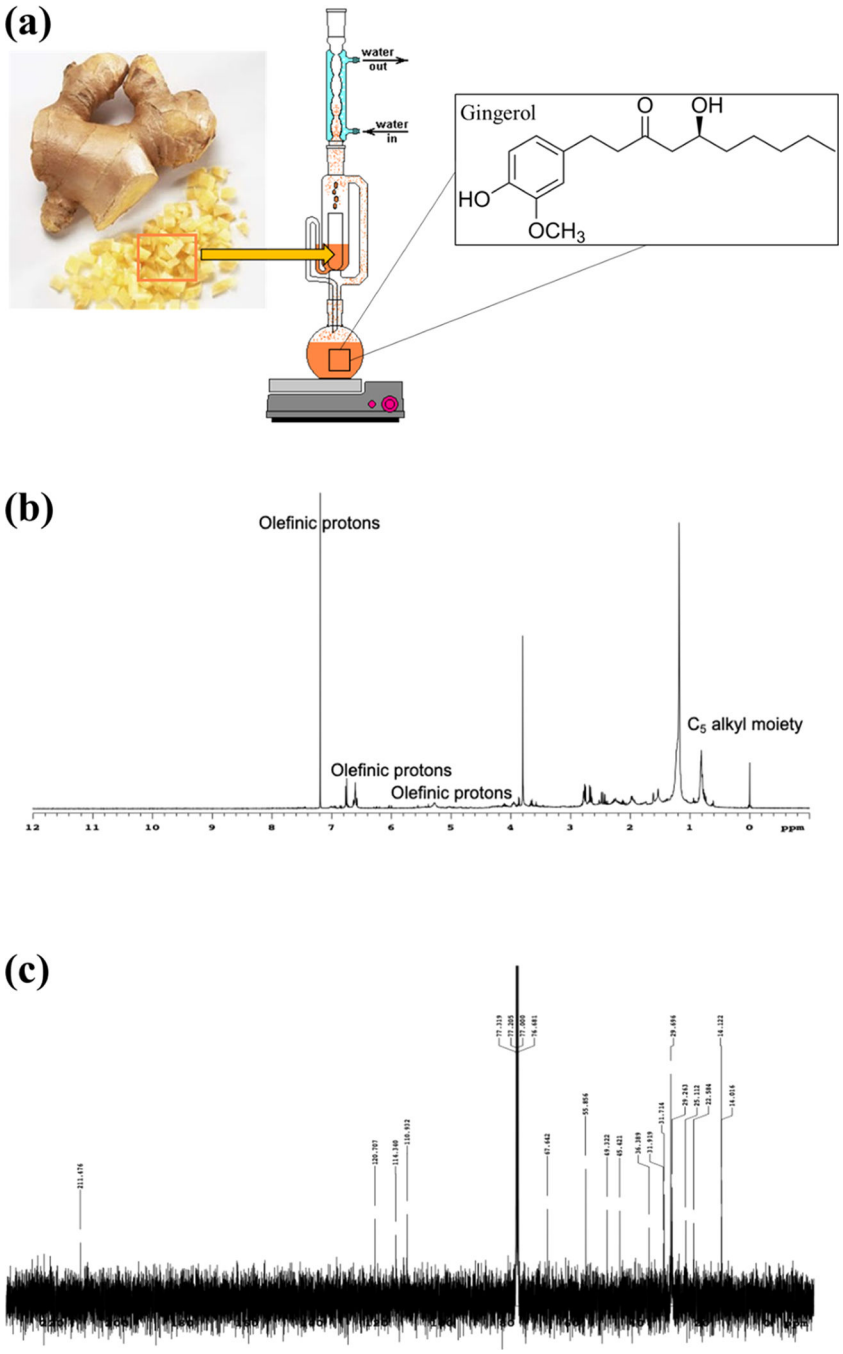

Figure 2.

Ginger extraction and NMR characterization. (a) Schematic of Soxhlet extraction of extract from the ginger root. (b) ^{1}H NMR spectrum of ginger extraction showing olefinic protons and the C_5 alkyl moiety. (c) ^{13}C NMR spectrum of ginger extraction demonstrating the presence of isomers of gingerol.

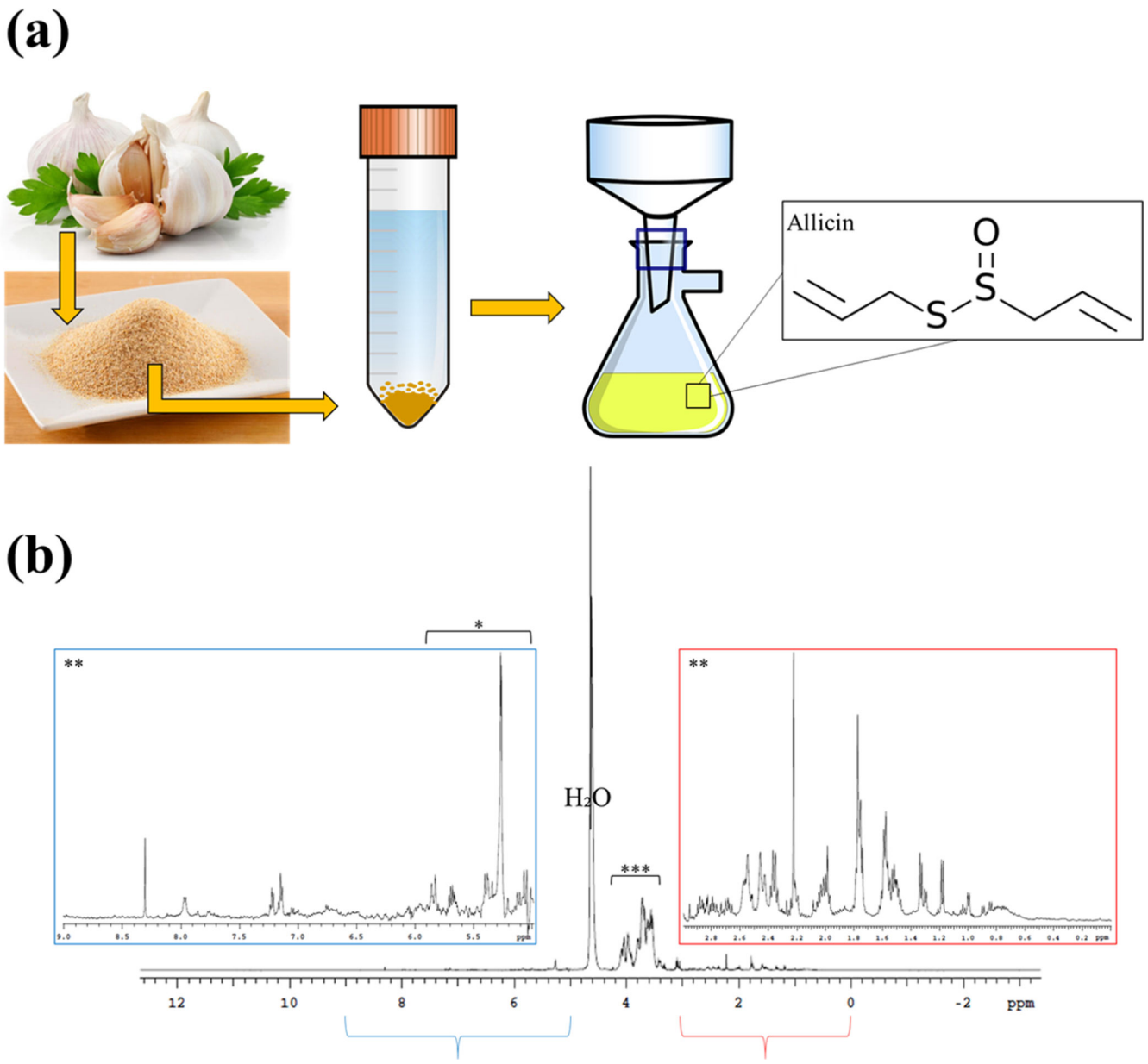

Figure 3.

Garlic extraction and NMR characterization. (a) Schematic of garlic extraction using garlic powder. (b) ^{1}H NMR spectrum of garlic extraction showing characteristic peaks of organosulfur compounds such as allicin.

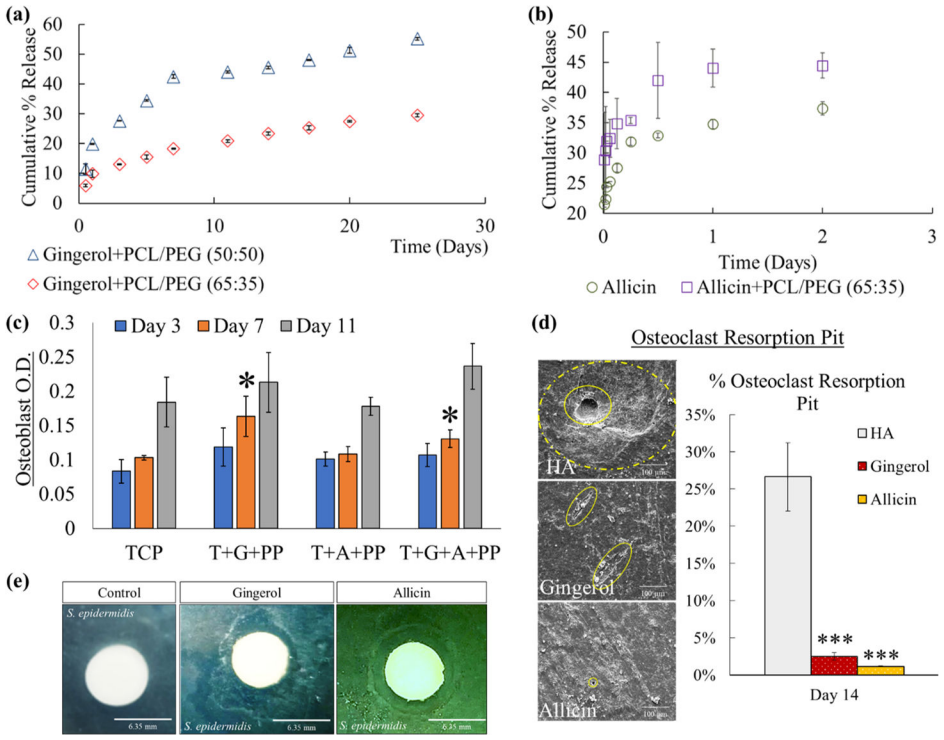

Figure 4.

In vitro drug release and cell materials interaction with osteoblast, osteoclast, and *S. epidermidis* cells. (a) Ginger extract (gingerol) release shows an exponential release following a Weibull distribution. (b) Garlic extract shows ~35% total release without PCL/PEG and 45% with polymer, also following a Weibull distribution. (c) MTT cell viability quantification assay identifies osteoblast optical density (OD) under UV analysis with no cytotoxicity among all compositions compared to control TCP. Also seen is an enhanced osteoblast proliferation with samples loaded with ginger extract at day 7 compared to the control (*, $n = 3$, $p < 0.05$). (d) Osteoclast resorption pits show less-severe resorption and flattened pits with ginger and garlic extract-loaded samples compared to control HA. Surface area quantification reveals a statistical decrease in osteoclast resorption pit (***, $n = 3$, $p < 0.001$). (e) Ginger and garlic extract solutions show antibacterial properties against *S. epidermidis* bacteria seen by the zone of inhibition of 9.9 ± 1.3 and 9.7 ± 0.1 mm, respectively, around the white disc. Control disc shows no zone of inhibition.

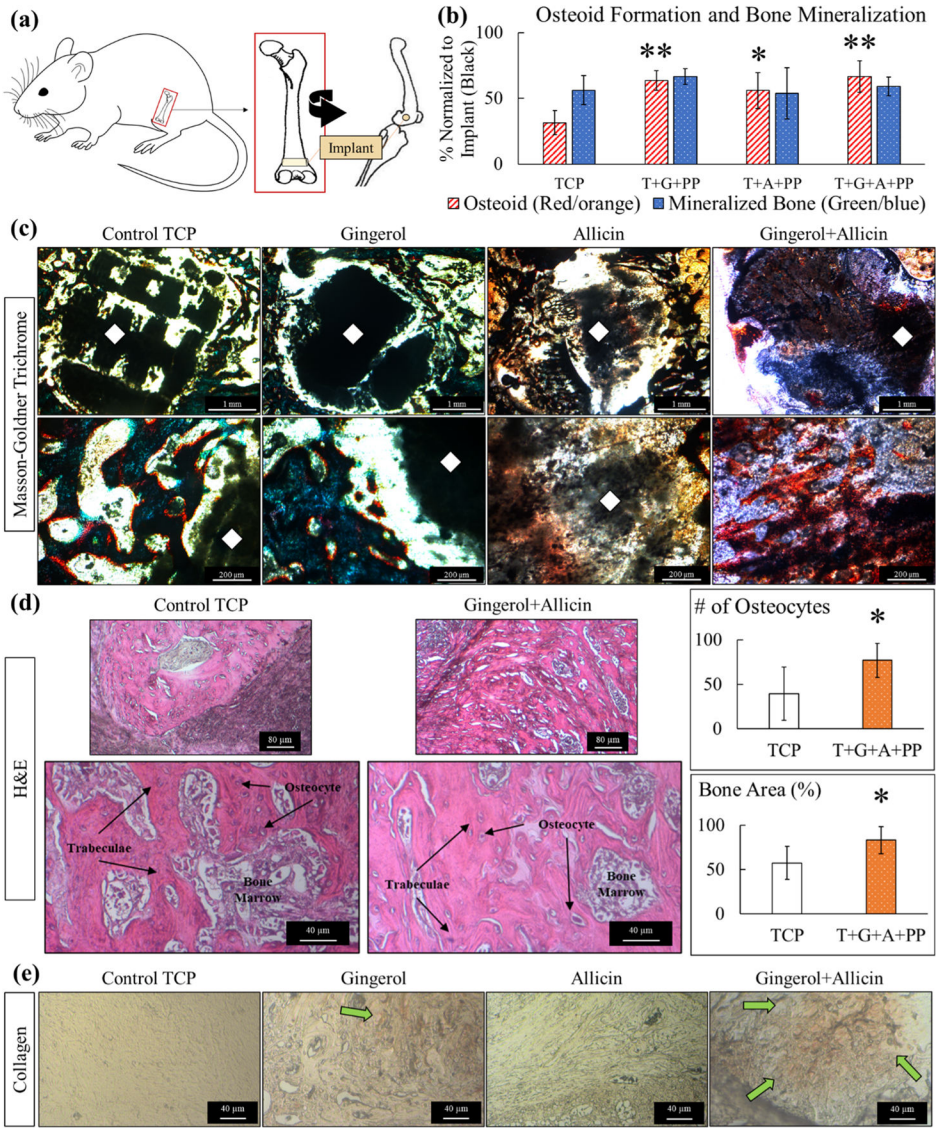

Figure 5.

Week 4 *in vivo* analysis. (a) Schematic representation of *in vivo* rat distal femur model surgery. (b) Histomorphometry of osteoid formation and bone mineralization, normalized to the exposed implant area (black). Ginger extract (gingerol), garlic extract (allicin), and ginger + garlic extract (gingerol + allicin) show a significantly higher formation of osteoid compared to control TCP ($n = 5$, $*p = 0.05$, and $**p = 0.01$). (c) Optical microscopy images of quantified Masson-Goldner trichrome staining show prominent osteoid formation of ginger + garlic extract samples compared to the control. Color coding is as follows: implant (black marked with a white diamond), osteoid tissue (red/orange), and mineralized bone tissue (green/blue). Gaps in tissue growth are seen within control TCP scaffold implants at both timepoints comparatively to ginger + garlic extract-loaded TCP scaffolds. (d) H&E-stained tissues show healthy bone tissue, trabecular bone tissue, osteocytes, and bone marrow in all compositions. Ginger and garlic extracts both individually show support of osteogenesis, but results are more profound when they are used together. Ginger + garlic

extract supports about a 90% increase in osteocytes and 30% increase in bone area (*, $n = 5$, $p < 0.05$). (e) Collagen staining shows an increase in collagen formation with ginger extract and even more so by ginger + garlic extract scaffolds in week 4. Collagen is indicated by the orange/yellow color and green arrow. Enhanced type I collagen can induce osteoblastic differentiation, thus aiding in osteogenesis and bone healing.

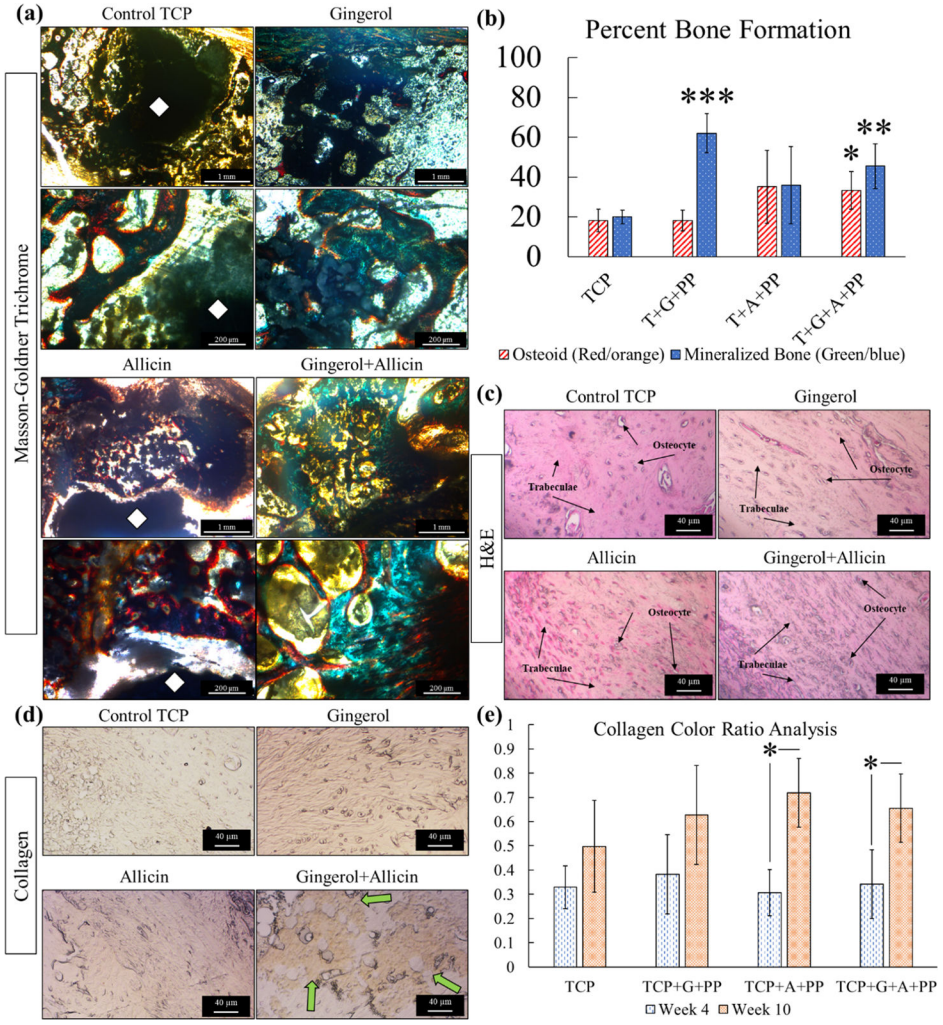

Figure 6.

Week 10 *in vivo* analysis. (a) Histomorphometry of osteoid formation and bone mineralization, normalized to the exposed implant area (black). Ginger + garlic extract (gingerol + allicin) shows a significantly higher formation of osteoid and bone mineralization compared to control TCP. Ginger extract also shows significant bone mineralization compared to control TCP ($n = 5$, $*p = 0.05$, $**p = 0.01$, and $***p < 0.001$). (b) Optical microscopy images of modified Masson-Goldner trichrome staining show higher mineralized bone formation with ginger + garlic extract scaffolds compared to the control. Ginger + garlic extract scaffolds became indistinguishable due to high tissue in-growth, whereas gaps are still seen in control TCP scaffold implants. (c) H&E staining shows healthy trabecular tissue with osteocytes in all samples. (d) Collagen staining reveals that ginger + garlic extract supports prominent collagen formation compared to all compositions. (e) Collagen color analysis of week 4 and week 10 stained tissues shows a significant increase in collagen formation at late-stage bone healing with garlic extract treatment.

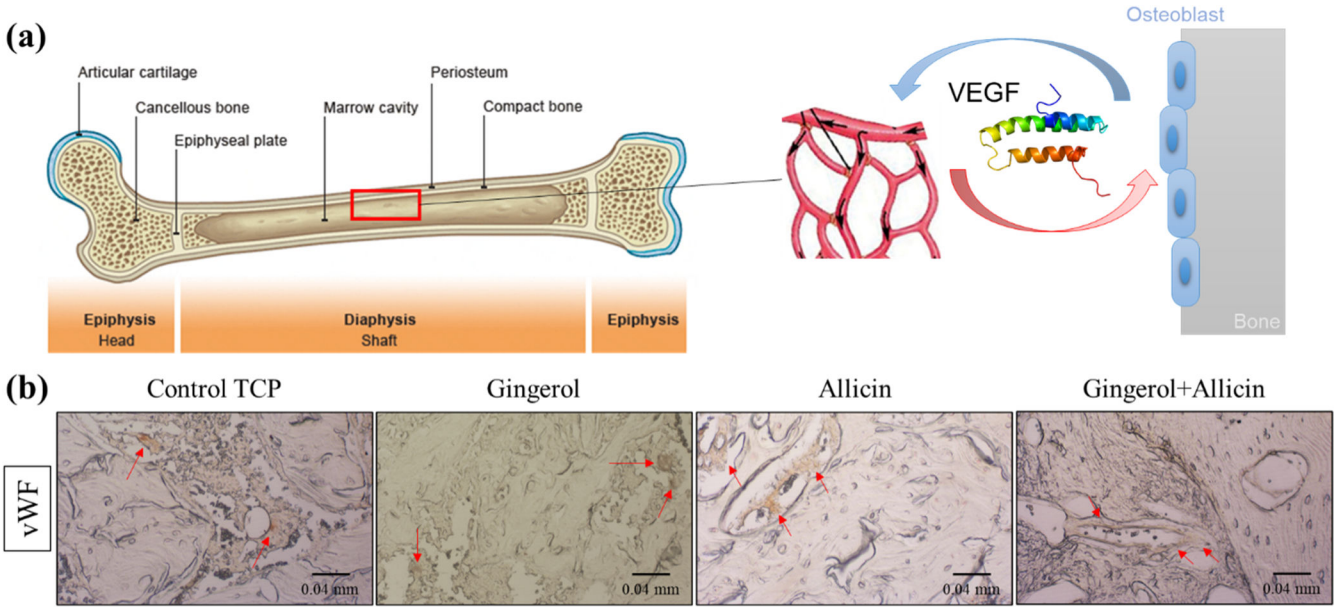

Figure 7.

Week 10 vWF staining. (a) Angiogenesis from VEGF protein signaling supports osteogenesis and bone formation. (b) Blood vessel stain using vWF tags several growth factors including VEGF. This staining of week 10 samples shows healthy angiogenic tissue across all control TCP and TCP compositions with ginger extract, garlic extract, and ginger + garlic extract. This indicates that ginger and garlic extracts individually and together can support necessary angiogenesis to facilitate bone tissue repair.